Inducing and controlling rotation on small objects using photonic topological materials

Lindel Frieder, George W. Hanson, Mauro Antezza, Stefan Yoshi Buhmann

Inducing and controlling rotation on small objects using photonic topological materials

Frieder Lindel,[1] George W. Hanson,[2] Mauro Antezza,[3,4] and Stefan Yoshi Buhmann[1,5]

[1]*Physikalisches Institut, Albert-Ludwigs-Universität Freiburg, Hermann-Herder-Straße 3, 79104 Freiburg, Germany*

[2]*Department of Electrical Engineering, University of Wisconsin–Milwaukee, 3200 N. Cramer Street, Milwaukee, Wisconsin 53211, USA*

[3]*Laboratoire Charles Coulomb, UMR 5221 Université de Montpellier and CNRS, 34095 Montpellier, France*

[4]*Institut Universitaire de France, 1 rue Descartes, 75231 Paris Cedex 5, France*

[5]*Freiburg Institute for Advanced Studies, Albert-Ludwigs-Universität Freiburg, Albertstraße 19, 79104 Freiburg, Germany*

(Received 19 March 2018; revised manuscript received 10 August 2018; published 1 October 2018)

Photonic topological insulator plates violate Lorentz reciprocity, which leads to a directionality of surface-guided modes. This in-plane directionality can be imprinted via an applied magnetic field. On the basis of macroscopic quantum electrodynamics in nonreciprocal media, we show that two photonic topological insulator surfaces are subject to a tunable, magnetic-field-dependent Casimir torque. Due to the directionality, this torque exhibits a unique 2π periodicity, in contradistinction to the Casimir torques encountered for reciprocal uniaxial birefringent media or corrugated surfaces which are π periodic. Remarkably, the torque direction and strength can be externally driven *in situ* by simply applying a magnetic field on the system, and we show that this can be exploited to induce a control of the rotation of small objects. Our predictions are relevant for nano-optomechanical experiments and devices.

DOI: 10.1103/PhysRevB.98.144101

I. INTRODUCTION

The Casimir force was originally proposed as an attractive force between two perfectly conducting plates due to a reduced virtual photon pressure in the space between the plates [1,2]. Subsequently, the Casimir force for objects consisting of anisotropic materials or possessing anisotropic surfaces like birefringent plates [3], magnetodielectric metamaterials [4], and corrugated metals [5] was studied. Since all those materials have a distinguishable axis in the plane of the plates, it is natural to ask whether the Casimir energy depends on the relative angle between the two axes when bringing two anisotropic surfaces together. It turns out that, indeed, one obtains a Casimir torque [3,5–9]. There have been successful measurements of the lateral Casimir force, which is closely related to the Casimir torque [10–14]. More recently, there also have been several promising proposals for experiments with the goal to measure the Casimir torque between birefringent materials [15–17].

A material which is able to break rotational symmetry and which is of great interest at the moment is the topological insulator (TI) [18]. Topological insulators behave like regular insulators in their bulk but possess conducting surface states. Originally proposed for electronic states, it was shown more recently that they also exist in so-called photonic topological insulators (PTIs) [19–22] such as magnetized plasma [23–25]. One of the most striking features of TIs is that there exist unidirectional waves on the surfaces of these materials which turn out to be immune to backscattering [26,27]. Due to this directionality of the edge states PTIs not only have a distinguishable axis like, e.g., birefringent materials, but their axes also possess a distinguished *direction*. This feature has been of great interest and was used to construct devices like directional wave guides [27], optical isolators, and circulators.

Now the natural question arises regarding what quantum optical effects emerge when exploiting the directionality or nonreciprocity in PTIs. This question has been addressed by previous authors before: they studied the influence of the presence of a PTI on the entanglement of a two-level system [28]. In Refs. [29–31] the normal and lateral Casimir-Polder force acting on an atom close to a vacuum/PTI interface was analyzed; a huge anisotropic thermal magnetoresistance was obtained in the near-field radiative heat transfer between two spherical particles consisting of a PTI in Ref. [32]. A persistent unidirectional heat current was found between three objects at thermal equilibrium [33,34]; also the Casimir force has been studied for two infinite half-spaces consisting of PTIs in Ref. [35]. All those works showed that there exist interesting new features in quantum optics arising from the interplay of the quantized electromagnetic field with PTIs. However, the unidirectional features of PTIs have not yet been seen to manifest in Casimir torques between two macroscopic objects.

II. CASIMIR TORQUE

In this paper, we want to show how the unidirectionality and nonreciprocity of PTI plates manifest in the Casimir force and torque. To this end, we will show in the following that, in addition to a normal component of the Casimir force, there exists a non-negligible Casimir torque whose magnitude and direction are tunable by the external magnetic fields. Furthermore, due to the directionality of the topological surface states, we find that this torque is 2π periodic with respect to the relative angle between the two bias magnetic fields, in sharp contrast to the π periodicity occurring for reciprocal bianisotropic media. We also discuss how the tunability of the Casimir torque can be exploited in nanomechanical schemes to induce rotation.

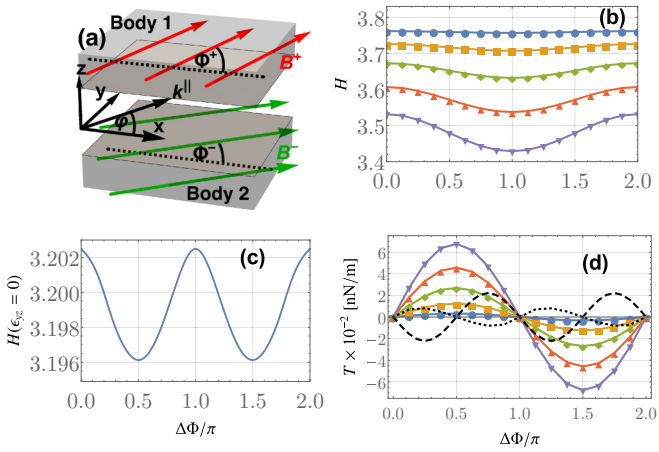

FIG. 1. In (a) we show the setup under the consideration consisting of two semi-infinite half-spaces filled with a PTI. Additionally, in each half-space there is an applied external magnetic field $\mathbf{B}^+$ and $\mathbf{B}^-$. The fields are in the xy plane and are parametrized by the angles Φ^+ and Φ^- between $\mathbf{B}^+$ and $\mathbf{B}^-$ and the x axis, respectively. In (b) we plot the dimensionless Hamaker constant H as a function of $\Delta\Phi$ for different values of $B = 1, 2, 3, 4, 5$ T (dots, squares, diamonds, triangles, and upside-down triangles, respectively). In (c) we again use the $\boldsymbol{\epsilon}$ tensor in Eq. (1) with the only exception being that we set $\epsilon_{yz} = 0$ to obtain a description of a normal anisotropic medium ($B = 5$ T). The Casimir torque $T(\Delta\Phi)$ is plotted in (d) for different magnetic fields, where the same shapes correspond to the same values of B as in (b). Additionally, we plot the Casimir torque for the material model in (c) (dotted line) and for a setup where the two PTI half-spaces are replaced by one barium titanate and one quartz half-space (dashed line). In (b) and (c) we use $L = 100$ nm.

A. Setup

We study a setup consisting of two semi-infinite half-spaces separated by a vacuum with separation L and filled with PTIs where a bias magnetic field is applied to each half-space [see Fig. 1(a)]. The PTI is implemented by a magnetized plasma with an applied bias magnetic field $\mathbf{B}$ as an example of a gyrotropic material which is described by a permittivity tensor of the form [36]

$$\boldsymbol{\epsilon} = \begin{pmatrix} \epsilon_{xx} & 0 & 0 \\ 0 & \epsilon_{zz} & \epsilon_{yz} \\ 0 & -\epsilon_{yz} & \epsilon_{zz} \end{pmatrix},$$
$$\epsilon_{yz}(\omega) = \frac{i\omega_c\omega_p^2}{\omega\left[\omega_c^2 - (\omega + i\gamma)^2\right]},$$
$$\epsilon_{zz}(\omega) = 1 + \frac{\omega_L^2 - \omega_T^2}{-i\Gamma\omega + \omega_T^2 - \omega^2} + \frac{\omega_p^2(\omega + i\gamma)}{\omega\left[\omega_c^2 - (\omega + i\gamma)^2\right]}, \tag{1}$$
$$\epsilon_{xx}(\omega) = 1 + \frac{\omega_L^2 - \omega_T^2}{-i\Gamma\omega + \omega_T^2 - \omega^2} - \frac{\omega_p^2}{\omega(\omega + i\gamma)}$$

if $\mathbf{B}$ points in the x direction. This is easily generalized for arbitrary directions of the magnetic field by simply rotating $\boldsymbol{\epsilon}$. The plasma and cyclotron frequencies are given by $\omega_p = \sqrt{nq_e^2/(m^\star\epsilon_0)}$ and $\omega_c = Bq_e/m^\star$, respectively, where q_e is the electron charge, $m^\star$ is its reduced mass, n is the free-electron density, and γ is the free-carrier damping constant. Furthermore, Γ represents the phonon damping constant, and ω_L and ω_T are the longitudinal and transverse optic-phonon frequencies, respectively. Throughout this paper we will use the following values for the material constants of InSb which have been measured in Ref. [36]: $\omega_L = 3.62 \times 10^{13}$ rad/s, $\omega_T = 3.39 \times 10^{13}$ rad/s, $\Gamma = 5.65 \times 10^{11}$ rad/s, $\gamma = 3.39 \times 10^{12}$ rad/s, $n = 1.07 \times 10^{17}\,\mathrm{cm}^{-3}$, $m^\star = 0.022m_e$, where m_e is the electron mass. Although we choose a specific PTI model here, our findings are general and can be applied to other specific PTI realizations.

B. Basic formulas

We first have to derive a general expression for the Casimir torque T of our system which is usually obtained from the Casimir energy E of the system. To build on previous results we use the intermediate result in Eq. (18) of Ref. [35] as obtained using macroscopic QED in nonreciprocal media [37]:

$$\mathbf{F} = -\frac{\hbar}{2\pi}\int_0^\infty d\xi \int_{\partial V} d\mathbf{A}\left\{\frac{2\xi^2}{c^2}\mathscr{S}[\mathbf{G}^{(1)}(\mathbf{r},\mathbf{r}',i\xi)] + 2\nabla\times\mathscr{S}[\mathbf{G}^{(1)}(\mathbf{r},\mathbf{r}',i\xi)]\times\overleftarrow{\nabla}'\right.$$
$$\left. -\mathrm{Tr}\left[\frac{\xi^2}{c^2}\mathbf{G}^{(1)}(\mathbf{r},\mathbf{r}',i\xi) + \nabla\times\mathbf{G}^{(1)}(\mathbf{r},\mathbf{r}',i\xi)\times\overleftarrow{\nabla}'\right]\mathbf{I}\right\}_{\mathbf{r}'\to\mathbf{r}}. \tag{2}$$

Here we have introduced the symmetrization $\mathscr{S}$ of a tensor defined by $\mathscr{S}[\mathbf{G}(\mathbf{r},\mathbf{r}',\omega)] = (1/2)[\mathbf{G}(\mathbf{r},\mathbf{r}',\omega) + \mathbf{G}^{\mathrm{T}}(\mathbf{r}',\mathbf{r},\omega)]$. Furthermore, $\xi = -i\omega$, where ω is the frequency of the electromagnetic wave, $\mathbf{I}$ is the unit tensor, ∂V is any infinite planar surface in the vacuum gap between the two planar bodies, $d\mathbf{A}$ is its surface element, and $\mathbf{r}$ and $\mathbf{r}'$ are arbitrary points on the surface of body 1. Most importantly, $\mathbf{G}^{(1)}(\mathbf{r},\mathbf{r}',i\xi)$ is the scattering Green's tensor [38] of our setup. It can be expressed using the reflection coefficients of the vacuum/PTI interfaces calculated in Appendix A and the different components of the wave vector $\mathbf{k} = (\mathbf{k}^{\parallel,T}, k_z = i\kappa)^{\mathrm{T}}$ satisfying $\mathbf{k}^2 = -\xi^2/c^2$, where c is the speed of light in vacuum. The full expression of $\mathbf{G}^{(1)}(\mathbf{r},\mathbf{r}',i\xi)$ and its derivation can be found in Appendix A.

Using these results, we find first of all, as expected, that there is no lateral force in the ground state of the system, and thus the x and y components of $\mathbf{F}$ are zero. Furthermore, in Appendix B we find a general expression for the normal component of $\mathbf{F}$ per unit area A which we define as $f \equiv F_z/A$, where F_z is the z component of $\mathbf{F}$. This result is not shown here since we are interested only in the near-field behavior of our system. Thus we want to analyze f further under

the assumption $\xi/c \ll k^{\parallel}$, which is often referred to as the nonretarded limit and becomes valid for small separations $L \ll c/\omega_{\rm ch}$, where $\omega_{\rm ch}$ is the highest characteristic frequency of the permittivity tensor (compare Ref. [38]). To estimate the value of $\omega_{\rm ch}$ for our specific material model in Eq. (1) we take a closer look at the monotonically decreasing function $\chi_{ij}(i\xi)/[\chi_{ij}(i\xi)+2]$, with $\chi_{ij}(i\xi) = \epsilon_{ij}(i\xi) - \delta_{ij}$. The condition

$$\frac{\chi_{ij}(i\omega_{\rm ch})}{\chi_{ij}(i\omega_{\rm ch})+2} = \frac{1}{2} \tag{3}$$

gives a good estimate of the characteristic frequency $\omega_{\rm ch}$. Neglecting absorption effects and phonon contributions. one obtains from Eq. (3)

$$ij = xx,\ zz \Rightarrow \omega_{\rm ch} \simeq \frac{\omega_p}{\sqrt{2}}, \tag{4}$$

$$ij = yz \Rightarrow \omega_{\rm ch} \simeq \sqrt[3]{\omega_p \omega_c}, \tag{5}$$

where we also assumed $\omega_c \ll \omega_p$, which is true for magnetic fields B of the order of a few teslas. Therefore we conclude that the nonretarded limit approximation is valid for distances $L \ll c\sqrt{2}/\omega_{\rm p} = 3.4\,\mu$m. Note, however, that this estimation for the validity of the nonretarded limit approximation is true only for our specific material model as given in Eq. (1), which includes only two medium resonances.

Under this assumption the reflection coefficients simplify significantly to $r^{\pm}_{\rm s,s} \simeq r^{\pm}_{\rm s,p} \simeq r^{\pm}_{\rm s,p} \simeq 0$ and

$$r^{\pm}_{\rm pp}(\omega) \simeq \frac{-2 + D \mp 2i\epsilon_{yz}\sin(\Phi^{\pm}-\varphi)}{2 + D \mp 2i\epsilon_{yz}\sin(\Phi^{\pm}-\varphi)},$$
$$D = \sqrt{2\epsilon_{zz}\{\epsilon_{zz} + \epsilon_{\rm xx} + (\epsilon_{\rm xx} - \epsilon_{zz})\cos[2(\Phi^{\pm}-\varphi)]\}}. \tag{6}$$

Here φ is defined by $\mathbf{k}^{\parallel} = k^{\parallel}(\sin(\varphi), \cos(\varphi))^{\rm T}$, with $k^{\parallel} \equiv |\mathbf{k}^{\parallel}|$ [compare Fig. 1(a)], and the $\pm$ symbol indicates the reflection at the lower and upper half-spaces, respectively. Note that this reflection coefficient is not real even when evaluated at imaginary frequencies $\omega = i\xi$ due to the terms proportional to ϵ_{yz}. But since this term also flips sign under $\mathbf{k}^{\parallel} \to -\mathbf{k}^{\parallel}$, the Schwarz reflection principle $\mathbf{G}^{(1)}(\mathbf{r}, \mathbf{r}', i\xi) = \mathbf{G}^{(1)\star}(\mathbf{r}, \mathbf{r}', i\xi)$ is obeyed, which, according to [39], implies $r^{\star}_{\rm pp}(\mathbf{k}^{\parallel}, i\xi) = r_{\rm pp}(-\mathbf{k}^{\parallel}, i\xi)$. Thus it is ensured that the Green's tensor and therefore the Casimir force are real.

Finally, using the previous result of the reflection coefficients in the nonretarded limit, f simplifies to

$$f = -\frac{\hbar}{16\pi^3 L^3}\int_0^{\infty} d\xi \int_0^{2\pi} d\varphi\ {\rm Li}_3[r^{+}_{\rm pp}(i\xi) r^{-}_{\rm pp}(i\xi)], \tag{7}$$

where $\rm Li_3$ is the polylogarithm of order 3. As in the reciprocal case [38] and for a magnetized plasma with a bias magnetic field perpendicular to the interface [35], we find a simple $f \propto 1/L^3$ behavior in the nonretarded limit. Therefore we can easily calculate the Casimir energy E per unit area in the nonretarded limit from Eq. (B19) by integrating f with respect to L and eventually find $E = L\,f/2$. From this result we can now calculate the Casimir torque $T = -\partial E/(\partial\Delta\Phi)$, where $\Delta\Phi = \Phi^{-} - \Phi^{+}$.

III. RESULTS AND DISCUSSION

Next, we want to analyze our previous results for the Casimir force, energy, and torque. To this end, in Fig. 1(b), we display the dimensionless Hamaker constant defined by $H \equiv \int_0^{\infty}(d\xi/\omega_p)\int_0^{2\pi} d\varphi {\rm Li}_3[r^{+}_{\rm pp} r^{-}_{\rm pp}]$ at a fixed gap distance $L =$ 100 nm. Note that one can easily retrieve f, E, and T from H via $f = -\omega_p\hbar H/16\pi^3 L^3$, $E = -\omega_p\hbar H/32\pi^3 L^2$, and $T = (\omega_p\hbar/32\pi^3 L^2)\partial H/(\partial\Delta\Phi)$. Before discussing the qualitative features of these results let us discuss the magnitude of the torque. As depicted in Fig. 1(d), the Casimir torque at zero temperature for two semi-infinite PTI half-spaces reaches the same order of magnitude as the one for quartz or calcite half-spaces kept parallel to a barium titanate half-space. Those examples for birefringent plates were studied in Ref. [15], and we have used the same model for the permittivity, including the same values for the constants measured in Ref. [40] to reproduce these results. More concretely, this means that the torque for the PTI setup reaches a maximal torque of about 67 pN/m with $B = 5$ T, whereas the quartz (calcite)–barium titanate setup reaches 22 pN/m (317 pN/m). Nevertheless, the Casimir torque between two corrugated metals is three orders of magnitude larger [5]. Note that these torques are all periodic under a rotation of π of one of the plates around its normal component since their distinguished axes are not directional. On the contrary, we see in Fig. 1(b) that $H(\Delta\Phi)$ is 2π periodic with a maximum (minimum) when the two magnetic fields $B^{\pm}$ point in the same (opposite) direction. This result is therefore qualitatively different from the ones observed when dealing with birefringent half-spaces with one in-plane optical anisotropy [15] [compare the dashed line in Fig. 1(d)] or corrugated metals [5]. Heuristically, this new periodicity can be explained by the fact that not only does our material model have a distinguished axis, but this axis also has a direction.

The angle dependence of the Casimir energy can be understood in more detail by studying the contributions of different surface-plasmon polaritons (SPPs) which dominate in the nonretarded limit [41]. To this end, we take a closer look at the spectral decomposition of the Casimir energy evaluated at real frequencies $\tilde{H}(\omega) \equiv \int_0^{2\pi} d\varphi\ {\rm Im}\{{\rm Li}_3[r^{+}_{\rm pp}(\omega) r^{-}_{\rm pp}(\omega)]\}$, which allows us to see which surface modes contribute the most to the Casimir energy. The total Casimir energy is simply the integral over this spectral energy density, $H = \int_0^{\infty}(d\omega/\omega_p)\tilde{H}(\omega)$, and therefore $E, f \propto \int_0^{\infty} d\omega\ \tilde{H}(\omega)$, as can be seen from contour-integral techniques.

The central ingredient to the spectral Casimir energy density is the SPPs of the individual plates, which are resonances of the respective reflection coefficients $r^{+}_{\rm pp}(\omega)$ and $r^{-}_{\rm pp}(\omega)$. The frequencies of the SPPs are easily found by setting the denominators in the reflection coefficients (6) to zero, which upon using Eq. (1) and neglecting the photon contribution leads to the dispersion relations

$$\Omega^{\pm}(\Phi^{\pm}-\varphi) = \tfrac{1}{4}\Big\{\sqrt{6\omega_c^2 + 8\omega_p^2 + 2\omega_c^2\cos[2(\Phi^{\pm}-\varphi)]} \pm 2\omega_c\sin[\Phi^{\pm}-\varphi]\Big\} \tag{8}$$

in the lossless limit, as also found in Ref. [29]. The single-plate SPPs are illustrated by the dotted and dashed lines in

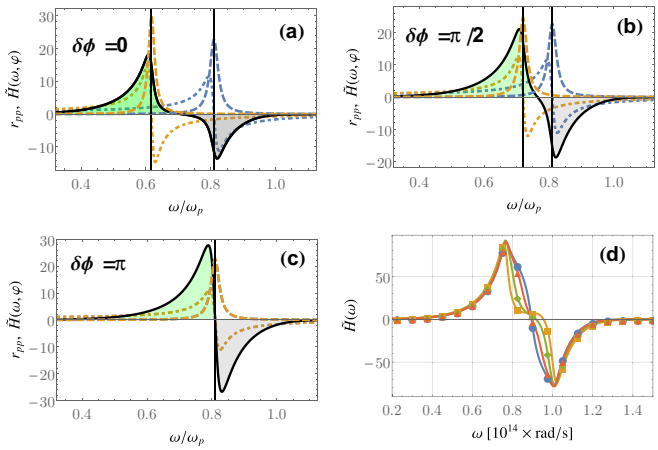

FIG. 2. Contributions of surface-plasmon polaritons (SPPs) to the Casimir energy. (a)–(c) Single-plate SPPs $\mathrm{Re}[r_{\mathrm{pp}}^{\pm}(\omega)]$ (dotted lines) and $\mathrm{Im}[r_{\mathrm{pp}}^{\pm}(\omega)]$ (dashed lines) and angle-resolved spectral energy density $\tilde{H}(\omega,\varphi)$ (solid lines) with $\Phi^{+}-\varphi=\pi/2$ and $\Delta\Phi=0,\pi/2,\pi$, respectively. $\mathrm{Re}[r_{\mathrm{pp}}^{+}(\omega)]$ and $\mathrm{Im}[r_{\mathrm{pp}}^{+}(\omega)]$ correspond to the curves with the resonance at higher frequencies, whereas $\mathrm{Re}[r_{\mathrm{pp}}^{-}(\omega)]$ and $\mathrm{Im}[r_{\mathrm{pp}}^{-}(\omega)]$ correspond to the ones with a lower resonance frequency ($\Omega^{+}>\Omega^{-}$ in this case); the two single-plate SPP frequencies $\Omega^{\pm}(\Phi^{\pm}-\varphi)$ as given by Eq. (8) are indicated as vertical lines. (d) Total spectral energy density $\tilde{H}(\omega)$ with $\Delta\Phi=0,\pi/4,\pi/2,\pi$ (dots, triangles, diamonds, and squares, respectively). For all plots we have used $B=3$ T.

Figs. 2(a)–2(c) for selected combinations of magnetic field and wave vector directions. In particular, we see that the SPP frequencies of the two plates coincide in the special case $\Delta\Phi=\pi$ [Fig. 2(c)].

When the two plates are brought in close proximity, as is the case in the nonretarded limit considered, the single-plate SPPs combine to form symmetric and antisymmetric coupled SPPs [41]. Mathematically, this can be seen from the Casimir spectral energy density. Using $\mathrm{Li}_3[z]\approx\zeta(3)\,z$ for $z\ll 1$, where ζ is the Riemann zeta function, we find $\tilde{H}(\omega)\approx\zeta(3)\{\mathrm{Im}[r_{\mathrm{pp}}^{+}(\omega)]\mathrm{Re}[r_{\mathrm{pp}}^{-}(\omega)]+\mathrm{Im}[r_{\mathrm{pp}}^{-}(\omega)]\mathrm{Re}[r_{\mathrm{pp}}^{+}(\omega)]\}$. We can clearly see how $H(\omega,\varphi)$ is built up from the products $\mathrm{Im}[r_{\mathrm{pp}}^{\pm}(\omega)]\mathrm{Re}[r_{\mathrm{pp}}^{\mp}(\omega)]$ in Figs. 2(a)–2(c). As illustrated by the solid lines in Figs. 2(a)–2(c), the symmetric coupled SPPs give the dominant positive contribution to the Casimir energy (left peak), while the antisymmetric coupled SPPs give a smaller negative contribution (right dip). As further seen in the figures, the difference between the positive and negative contributions is quite pronounced for $\Delta\Phi=0$ [Fig. 2(a)], leading to a large net Casimir energy. The splitting is reduced for larger angles [Fig. 2(b)] until, eventually, the single-plate SPPs coincide for $\Delta\Phi=\pi$ and the two coupled SPPs become very close in frequency and similar in magnitude. For this case, we have a smaller Casimir energy.

Our observations remain valid for general combinations of magnetic field and wave vector directions and thus also when integrating over all wave vector directions $\varphi\in[0,2\pi]$ to obtain the total spectral energy density $\tilde{H}(\omega)$. As seen from Fig. 2(d), this energy density has quite a complex profile as it is the sum over contributions from many SPPs with different resonant frequencies. Nevertheless, we again find that positive and negative contributions are the most different in magnitude for $\Delta\Phi=0$ (dots), leading to a large total Casimir energy. As the angle difference increases towards $\Delta\Phi=\pi$ (squares), the positive and negative contributions become more similar in magnitude, and the total Casimir energy decreases.

IV. APPLICATION

The advantage of having an *in situ* tunability of the torque can be exploited for nanomechanical schemes. For instance, we consider a setup of two nanodisks as depicted in Fig. 3(a). This system is an example of a new mechanism (compare Ref. [47]) to generate a motor with small moving parts. As shown, the relative angle between the two applied magnetic fields is given by $\Delta\Phi(t)=\Phi^{-}(t)-\theta(t)$. The dependence of the torque T on the relative angle between the applied magnetic fields is well approximated by $T(\Delta\Phi)\cong T_0\sin(\Delta\Phi)$ [compare Fig. 1(d)], where $T_0=67\,\mathrm{pN/m}$ if $B^{+}=B^{-}=5$ T. Thus the equation of motion for the rotation of the upper disk neglecting finite-size effects, retardation, and friction is given by

$$\frac{d^2\theta}{dt^2}=\frac{2T_0}{lr^2\rho_{\mathrm{InSb}}}\sin[\Phi^{-}(t)-\theta(t)]. \tag{9}$$

The result of the numerical solution of Eq. (9) can be found in Fig. 3(b). As we can see, if we let the tunable magnetic field $\mathbf{B}^{-}$ rotate with an angular velocity of up to 0.75 rad/s, the upper plate will follow the direction of $\mathbf{B}^{-}$ and start to rotate with the same angular velocity of almost one full 2π rotation per second. If $\mathbf{B}^{-}$ rotates faster than 0.75 rad/s, the

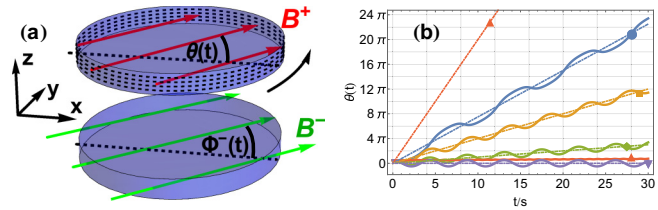

FIG. 3. (a) Scheme for inducing rotation via Casimir torques. As shown, there are two disks with the same size as considered in Ref. [16], namely, with radius $r=20\,\mu$m and thickness $d=20\,\mu$m consisting of InSb, which has a mass density of $\rho_{\mathrm{InSb}}=5.59\,\mathrm{g/cm^3}$ [42]. They are held at a distance of $L=100$ nm from each other so that the nonretarded limit assumption and the assumption of having two semi-infinite half-spaces apply for the idealized medium response assumed. Furthermore, $\mathbf{B}^{+}$ is a static magnetic field which is attached to the disk, i.e., via magnetic coating [43–46]. Thus its angle with the x axis Φ^{+} only changes if the whole disk rotates and the rotation of the upper disk is described by the angle $\theta(t)\equiv\Phi^{+}(t)$. In the lower disk there is a magnetic field $\mathbf{B}^{-}$ whose direction described by the angle $\Phi^{-}(t)$ may change over time, although the plate is fixed. In (b) we show the numerical solution to Eq. (9) with $B^{+}=B^{-}=5$ T for the cases $\Phi^{-}(t)=0.75\pi t, 0.4\pi t, 0.1\pi t, 2\pi t, 0$ (dot, square, diamond, triangle, and upside-down triangle, respectively) with solid lines. Additionally, we plot $\Phi^{-}(t)=0.75\pi t, 0.4\pi t, 0.1\pi t, 2\pi t, 0$ (also indicated by the dot, square, diamond, triangle, and upside-down triangle, respectively) describing the rotation of $\mathbf{B}^{-}$ with dot-dashed lines.

upper disk cannot follow the direction of $\mathbf{B}^-$, and therefore it barely rotates (triangle). Here r and l are the radius of the upper disk and its thickness, respectively.

V. SUMMARY

To summarize, we have found a Casimir torque between topological-insulator plates whose direction and magnitude are tunable by an external bias magnetic field. We have further shown that in the nonretarded limit this torque is dominated by SPPs which are directional, and therefore it is symmetric only under a rotation of 2π of one of the plates around its normal component. This unique periodicity, in contrast to the typical π periodicity for ordinary birefringent media, is a clear signature of nonreciprocity. We have shown how the tunability of the torque between two InSb disks can be exploited to set one of the disks into rotation, which offers new possibilities for measurements and nanomechanical applications of the Casimir torque on small objects.

ACKNOWLEDGMENTS

We acknowledge helpful discussions with F. Intravaia and A. Belyanin. This work was supported by the German Research Foundation (DFG, Grants No. BU 1803/3-1 and No. GRK 2079/1). S.Y.B. is grateful for support from the Freiburg Institute of Advanced Studies (FRIAS).

APPENDIX A: GREEN'S TENSOR FOR TWO SEMI-INFINITE HALF-SPACES OF PTI

In this appendix, we derive an expression for the Casimir force between two half-spaces filled with photonic topological materials separated by vacuum and with distinct in-plane bias magnetic fields in each of the half-spaces [see Fig. 1(a)]. To this end, we first calculate the Green's tensor for this setup here as the essential ingredient for the Casimir force calculated in Appendix B.

The following derivation of the Green's tensor $\mathbf{G}^{(1)}(\mathbf{r}, \mathbf{r}', \omega)$ is very similar to the ones given in Refs. [4,35]. As a starting point we can use the intermediate result of Ref. [35] in their Eq. (26):

$$\begin{aligned}\mathbf{G}^{(1)}(\mathbf{r}, \mathbf{r}', \omega) = \frac{i}{8\pi^2}\int d^2k^{\parallel}\frac{1}{k_z}e^{i\mathbf{k}^{\parallel}\cdot(\mathbf{r}-\mathbf{r}')}\Big[&e^{ik_z(z+z')}(\mathbf{e}_{s+},\ \mathbf{e}_{p+})\cdot\mathscr{R}^-\cdot(\mathscr{D}^+)^{-1}\cdot\begin{pmatrix}\mathbf{e}_{s-}\\ \mathbf{e}_{p-}\end{pmatrix}\\ &+e^{2ik_zL}e^{-ik_z(z+z')}(\mathbf{e}_{s-},\ \mathbf{e}_{p-})\cdot\mathscr{R}^+\cdot(\mathscr{D}^-)^{-1}\cdot\begin{pmatrix}\mathbf{e}_{s+}\\ \mathbf{e}_{p+}\end{pmatrix}\\ &+e^{2ik_zL}e^{ik_z(z-z')}(\mathbf{e}_{s+},\ \mathbf{e}_{p+})\cdot\mathscr{R}^-\cdot(\mathscr{D}^+)^{-1}\cdot\mathscr{R}^+\cdot\begin{pmatrix}\mathbf{e}_{s+}\\ \mathbf{e}_{p+}\end{pmatrix}\\ &+e^{2ik_zL}e^{-ik_z(z-z')}(\mathbf{e}_{s-},\ \mathbf{e}_{p-})\cdot\mathscr{R}^+\cdot(\mathscr{D}^-)^{-1}\cdot\mathscr{R}^-\cdot\begin{pmatrix}\mathbf{e}_{s-}\\ \mathbf{e}_{p-}\end{pmatrix}\Big].\end{aligned} \tag{A1}$$

Here we have split the wave vector $\mathbf{k} = (\mathbf{k}^{\parallel,T}, k_z)^{\mathrm{T}}$ into its components parallel ($\mathbf{k}^{\parallel}$) and perpendicular (k_z) to the plates, and the polarization vectors $\mathbf{e}_{s\pm}$, $\mathbf{e}_{p\pm}$ and the multiple reflection matrices $\mathscr{D}^{\pm}$ are defined by

$$\mathbf{e}_{s\pm} = \mathbf{e}_{k^{\parallel}} \times \mathbf{e}_z = \frac{1}{k^{\parallel}}\begin{pmatrix}k_y\\ -k_x\\ 0\end{pmatrix}, \tag{A2}$$

$$\mathbf{e}_{p\pm} = \frac{1}{k}(k^{\parallel}\mathbf{e}_z \mp k_z\mathbf{e}_{k^{\parallel}}) = \frac{1}{k}\begin{pmatrix}\mp\frac{k_z}{k^{\parallel}}k_x\\ \mp\frac{k_z}{k^{\parallel}}k_y\\ k^{\parallel}\end{pmatrix}, \tag{A3}$$

$$(\mathscr{D}^{\pm})^{-1} = \sum_{n=0}^{\infty}\left(\mathscr{R}^{\pm}\cdot\mathscr{R}^{\mp}e^{2ik^{\perp}L}\right)^n = \left[1-\mathscr{R}^{\pm}\cdot\mathscr{R}^{\mp}e^{2ik^{\perp}L}\right]^{-1}. \tag{A4}$$

We are left with the task of calculating the reflection matrices

$$\mathscr{R}^{\pm} = \begin{pmatrix}r^{\pm}_{s,s} & r^{\pm}_{s,p}\\ r^{\pm}_{p,s} & r^{\pm}_{p,p}\end{pmatrix} \tag{A5}$$

to find $\mathbf{G}^{(1)}(\mathbf{r}, \mathbf{r}', \omega)$. Here $r^{+}_{\sigma\sigma'}$ ($r^{-}_{\sigma\sigma'}$) is the reflection coefficient for a σ'-polarized incoming wave which is reflected off body 1 (body 2; see Fig. 1 in the main text) as a σ-polarized wave.

We are going to calculate $\mathscr{R}^+$ first and retrieve $\mathscr{R}^-$ from symmetry considerations. To find $\mathscr{R}^+$ we first find appropriate expressions for the electric and magnetic fields in vacuum and in the PTI by making use of Maxwell's equations. Afterwards, we can obtain $\mathscr{R}^+$ from the continuity relations at the interface.

We start with the permittivity tensor for body 1, which is given by

$$\boldsymbol{\epsilon} = \begin{pmatrix}\epsilon_{xx} & 0 & 0\\ 0 & \epsilon_{zz} & \epsilon_{yz}\\ 0 & -\epsilon_{yz} & \epsilon_{zz}\end{pmatrix} \tag{A6}$$

if the external magnetic field $\mathbf{B}^+$ points in the x direction. Note that we have $\epsilon_{yy} = \epsilon_{zz}$ and $\epsilon_{yz} = -\epsilon_{zy}$. We generalize this expression to arbitrary directions Φ^+ of $\mathbf{B}^+$ (see Fig. 1 in the main text) in the xy plane by rotating $\boldsymbol{\epsilon}$ by an angle of Φ^+ around the z axes. Furthermore, we consider a general wave vector $\mathbf{k} = (k^{\parallel}\cos\varphi, k^{\parallel}\sin\varphi, k_z)^T$, but by rotating $\boldsymbol{\epsilon}$ by an angle of $-\varphi$ we get without loss of generality $\mathbf{k} = (k^{\parallel}, 0, k_z)^T$, which simplifies the following calculation

significantly. So the permittivity tensor eventually reads

$$\widetilde{\boldsymbol{\epsilon}} = \begin{pmatrix} \frac{1}{2}\{\epsilon_{xx}+\epsilon_{zz}+(\epsilon_{xx}-\epsilon_{zz})\cos[2(\Phi^+-\varphi)]\} & \frac{1}{2}(\epsilon_{xx}-\epsilon_{zz})\sin[2(\Phi^+-\varphi)] & -\epsilon_{yz}\sin[\Phi^+-\varphi] \\ \frac{1}{2}(\epsilon_{xx}-\epsilon_{zz})\sin[2(\Phi^+-\varphi)] & \frac{1}{2}\{\epsilon_{xx}+\epsilon_{zz}+(\epsilon_{zz}-\epsilon_{xx})\cos[2(\Phi^+-\varphi)]\} & \epsilon_{yz}\cos\left[\Phi^+-\varphi\right] \\ \epsilon_{yz}\sin[\Phi^+-\varphi] & -\epsilon_{yz}\cos[\Phi^+-\varphi] & \epsilon_{zz} \end{pmatrix} \tag{A7}$$

in the rotated frame. As expected, it depends on only the relative angle between the magnetic field and the wave vector. Note that this form of the permittivity tensor is different from the one considered in Ref. [35]. Nevertheless, the general procedure to find $\mathscr{R}^{\pm}$ is analogous.

Now we make a plane wave ansatz for the field in the vacuum layer given by

$$\begin{aligned} \mathbf{E}_{\mathrm{i}} &= \left[e_{\mathrm{s,i}}\mathbf{e}_y + e_{\mathrm{p,i}}\frac{c}{\omega\epsilon}(k_{z,\mathrm{i}}\mathbf{e}_x - k^{\parallel}\mathbf{e}_z)\right]e^{i(k^{\parallel}x+k_{z,\mathrm{i}}z-\omega t)}, \\ \mathbf{H}_{\mathrm{i}} &= \left[e_{\mathrm{p,i}}\mathbf{e}_y - e_{\mathrm{s,i}}\frac{c}{\omega}(k_{z,\mathrm{i}}\mathbf{e}_x - k^{\parallel}\mathbf{e}_z)\right]e^{i(k^{\parallel}x+k_{z,\mathrm{i}}z-\omega t)}, \\ \mathbf{E}_{\mathrm{r}} &= \left[e_{\mathrm{s,r}}\mathbf{e}_y - e_{\mathrm{p,r}}\frac{c}{\omega\epsilon}(k_{z,\mathrm{i}}\mathbf{e}_x + k^{\parallel}\mathbf{e}_z)\right]e^{i(k^{\parallel}x-k_{z,\mathrm{i}}z-\omega t)}, \\ \mathbf{H}_{\mathrm{r}} &= \left[e_{\mathrm{p,r}}\mathbf{e}_y + e_{\mathrm{s,r}}\frac{c}{\omega}(k_{z,\mathrm{i}}\mathbf{e}_x + k_x\mathbf{e}_z)\right]e^{i(k^{\parallel}x-k_{z,\mathrm{i}}z-\omega t)}, \end{aligned} \tag{A8}$$

which satisfies Maxwell's equations

$$\nabla\times\mathbf{E} = -\frac{1}{c}\frac{\partial}{\partial t}\mathbf{H}, \quad \nabla\times\mathbf{H} = \frac{1}{c}\frac{\partial}{\partial t}(\boldsymbol{\epsilon}\cdot\mathbf{E}), \tag{A9}$$

with $\boldsymbol{\epsilon} = \mathbf{I}$ since the wave propagates in vacuum. In Eq. (A8) $e_{\sigma,\mathrm{i}}$ and $e_{\sigma,\mathrm{r}}$ are unknown complex-valued amplitudes of the fields, where the subscripts i and r indicate the incident and reflected waves, respectively. To eventually find the reflection coefficients we also need to find a way to describe the field within the PTI. Due to the structure of $\widetilde{\boldsymbol{\epsilon}}$ in Eq. (A7) Maxwell's equations in Eq. (A9) mix s- and p-polarized waves within the PTI. Therefore an ansatz as in Eq. (A8) is not possible, and thus in a more general approach plane waves are assumed in the form

$$\mathbf{E} = \begin{pmatrix} e_x(z) \\ e_y(z) \\ e_z(z) \end{pmatrix}e^{i(k^{\parallel}x-\omega t)}, \quad \mathbf{H} = \begin{pmatrix} h_x(z) \\ h_y(z) \\ h_z(z) \end{pmatrix}e^{i(k^{\parallel}x-\omega t)}. \tag{A10}$$

Note that $k^{\parallel}$ is conserved across the interface. The z components of Maxwell's equations (A9) read

$$h_z(z) = \frac{c}{\omega}k^{\parallel}e_y(z), \tag{A11}$$

$$e_z(z) = \frac{1}{\epsilon_{zz}}\left[-\frac{c}{\omega}k^{\parallel}h_y(z) + \widetilde{\epsilon}_{xz}e_x(z) + \widetilde{\epsilon}_{yz}e_y(z)\right] \tag{A12}$$

and can be inserted into the x, y contributions. For these components we introduce the vector $\mathbf{u}$ with $u_1 = e_x$, $u_2 = e_y$, $u_3 = h_x$, and $u_4 = h_y$. By assuming the ansatz $u_j = u_j(0)e^{ik_z^{(m)}z}$ for the single components with $k_z^{(m)}$ as the z contribution of the wave vector in the PTI one obtains again from Eq. (A9)

$$\mathbf{L}\cdot\mathbf{u} = -\frac{c}{\omega}k_z^{(m)}\mathbf{u}, \tag{A13}$$

with

$$\mathbf{L} = \begin{pmatrix} -k^{\parallel}c\widetilde{\epsilon}_{\mathrm{xz}}/(\omega\widetilde{\epsilon}_{\mathrm{zz}}) & -k^{\parallel}c\widetilde{\epsilon}_{\mathrm{yz}}/(\omega\widetilde{\epsilon}_{\mathrm{zz}}) & 0 & -1+(ck^{\parallel}/\omega)^2 1/\widetilde{\epsilon}_{\mathrm{zz}}) \\ \widetilde{\epsilon}_{\mathrm{xy}}+\widetilde{\epsilon}_{\mathrm{yz}}\widetilde{\epsilon}_{\mathrm{xz}}/\widetilde{\epsilon}_{\mathrm{zz}} & \widetilde{\epsilon}_{\mathrm{yy}}+\widetilde{\epsilon}_{\mathrm{yz}}^2/\widetilde{\epsilon}_{\mathrm{zz}}-(\omega/ck^{\parallel})^2 & 0 & -\omega\widetilde{\epsilon}_{\mathrm{yz}}/(ck^{\parallel}\widetilde{\epsilon}_{\mathrm{zz}}) \\ -\tilde{\epsilon}_{xy} & \tilde{\epsilon}_{xx}-\frac{c^2}{\omega^2}(k^{\parallel})^2 & 0 & 0 \\ -\tilde{\epsilon}_{xx}-\widetilde{\epsilon}_{\mathrm{xz}}^2/\widetilde{\epsilon}_{\mathrm{zz}} & -\widetilde{\epsilon}_{xy}-\widetilde{\epsilon}_{\mathrm{yz}}\widetilde{\epsilon}_{\mathrm{xz}}/\widetilde{\epsilon}_{\mathrm{zz}} & 0 & \omega\widetilde{\epsilon}_{\mathrm{xz}}/(ck^{\parallel}\widetilde{\epsilon}_{\mathrm{zz}}) \end{pmatrix}. \tag{A14}$$

To find nontrivial solutions one has to solve the relation $\det[\mathbf{L}+\mathbf{I}\omega k_z^{(m)}/c] = 0$, leading to the dispersion relations

$$\begin{aligned} k_z^{(m)} &= \pm\frac{\omega}{c}\frac{1}{2l\sqrt{\epsilon_{zz}}}\sqrt{U_1+U_2\cos[2(\Phi^+-\varphi)] \pm \sqrt{\frac{1}{2}\{U_3+U_4\cos[2(\Phi^+-\varphi)]+U_2^2\cos[4(\Phi^+-\varphi)]\}}}, \\ U_1 &= -3\epsilon_{zz}+\epsilon_{xx}(2l^2\epsilon_{zz}-1)+2l^2\left(\epsilon_{yz}^2+\epsilon_{zz}^2\right), \quad U_2 = \epsilon_{zz}-\epsilon_{xx}, \\ U_3 &= 6\epsilon_{zz}^2-8l^2\,\epsilon_{zz}\left(\epsilon_{yz}^2+\epsilon_{zz}^2\right)+8l^4\left(\epsilon_{yz}^2+\epsilon_{zz}^2\right)^2+8l^2\,\epsilon_{zz}^3(\epsilon_{zz}l^2-1)-2\epsilon_{xx}\left[3\epsilon_{zz}+4l^2\left(\epsilon_{yz}^2-2\epsilon_{zz}^2\right)+8l^2\,\epsilon_{zz}\left(\epsilon_{yz}^2+\epsilon_{zz}^2\right)\right], \\ U_4 &= 4\left\{\epsilon_{xx}^2(1-2l^2\,\epsilon_{zz})-2\epsilon_{xx}\left[\epsilon_{zz}+l^2\left(\epsilon_{yz}^2-2\epsilon_{zz}^2\right)\right]+\epsilon_{zz}\left[\epsilon_{zz}-2l^2\left(\epsilon_{yz}^2+\epsilon_{zz}^2\right)\right]\right\} \end{aligned} \tag{A15}$$

for the four mathematical solutions $m = 1, 2, 3, 4$, corresponding to the possible combinations of signs in Eq. (A15) with the dimensionless quantity $l = \omega/(c\,k^{\parallel})$. Note that these dispersion relations agree with the ones found in Ref. [29]. Since solutions with $\mathrm{Im}[k^{\perp(m)}] > 0$ would result in waves propagating in the negative z direction, we can neglect these solutions for the transmitted wave propagating in the positive z direction. Let $k^{\perp(1)}$ and $k^{\perp(2)}$ be the two solutions with a positive real part; then neglecting the other two, we finally arrive at the expression for the transmitted components of $\mathbf{E}$ and $\mathbf{H}$ parallel to the surface,

$$\begin{pmatrix}\mathbf{E}_\mathrm{t}\\ \mathbf{H}_\mathrm{t}\end{pmatrix} = e^{i(k^{\parallel}x-\omega t)}\sum_{m=1,2}\mathbf{u}^{(m)}(0)e^{ik^{\perp(m)}z}. \tag{A16}$$

According to the continuity relations, the parallel components of the electric and magnetic fields $\mathbf{E}$ and $\mathbf{H}$, i.e., the x, y components, at the interface between vacuum and the topological insulator are continuous. To simplify this set of four equations we start by expressing e_y, h_x, and h_y in terms of e_x using Eqs. (A13) and (A14),

$$\begin{aligned}\alpha^{(m)} &\equiv \frac{e_y^{(m)}(0)}{e_x^{(m)}(0)} = \frac{(ck^{\perp(m)}/\omega + L_{11} - L_{31})L_{44}/L_{14}}{L_{32} - L_{12}\,L_{34}/L_{14} - (k^{\perp(m)}c/\omega)^2},\\ \beta^{(m)} &\equiv \frac{h_x^{(m)}(0)}{e_x^{(m)}(0)} = -\frac{-ck^{\perp(m)}}{\omega}\alpha^{(m)},\\ \gamma^{(m)} &\equiv \frac{h_y^{(m)}(0)}{e_x^{(m)}(0)} = \frac{-ck^{\perp(m)}/\omega - L_{11} - L_{12}\alpha^{(m)}}{L_{41}}.\end{aligned} \tag{A17}$$

These equations are inserted into the boundary conditions, and one obtains

$$\underbrace{\begin{pmatrix}-1 & 0 & \alpha^{(1)} & \alpha^{(2)}\\ \frac{ck_\mathrm{i}^{\perp}}{\omega} & 0 & -\beta^{(1)} & -\beta^{(2)}\\ 0 & \frac{ck_\mathrm{i}^{\perp}}{\omega} & 1 & 1\\ 0 & -1 & \gamma^{(1)} & \gamma^{(2)}\end{pmatrix}}_{\equiv\mathbf{M}}\begin{pmatrix}e_{\mathrm{s,r}}\\ e_{\mathrm{p,r}}\\ e_x^{(1)}\\ e_x^{(2)}\end{pmatrix} = \begin{pmatrix}e_{\mathrm{s,i}}\\ \frac{ck_\mathrm{i}^{\perp}}{\omega}e_{\mathrm{s,i}}\\ \frac{ck_\mathrm{i}^{\perp}}{\omega}e_{\mathrm{p,i}}\\ e_{\mathrm{p,i}}\end{pmatrix}. \tag{A18}$$

We now assume the incoming wave to be s ($e_{\mathrm{p,i}} = 0,\ e_{\mathrm{s,i}} \neq 0$) or p polarized ($e_{\mathrm{s,i}} = 0,\ e_{\mathrm{p,i}} \neq 0$) separately and solve for the reflected amplitudes to finally obtain the reflection coefficients with the help of Cramer's rule:

$$r_{\mathrm{s,s}}^{+} = \frac{e_{\mathrm{s,r}}}{e_{\mathrm{s,i}}} = \frac{\det(\mathbf{M}_1)}{\det(\mathbf{M})}, \tag{A19}$$

$$r_{\mathrm{p,s}}^{+} = \frac{e_{\mathrm{p,r}}}{e_{\mathrm{s,i}}} = \frac{\det(\mathbf{M}_2)}{\det(\mathbf{M})}, \tag{A20}$$

$$r_{\mathrm{s,p}}^{+} = \frac{e_{\mathrm{s,r}}}{e_{\mathrm{p,i}}} = \frac{\det(\mathbf{M}_3)}{\det(\mathbf{M})}, \tag{A21}$$

$$r_{\mathrm{s,s}}^{+} = \frac{e_{\mathrm{p,r}}}{e_{\mathrm{p,i}}} = \frac{\det(\mathbf{M}_4)}{\det(\mathbf{M})}, \tag{A22}$$

with the matrices

$$\mathbf{M}_1 = \begin{pmatrix}1 & 0 & \alpha^{(1)} & \alpha^{(2)}\\ \frac{ck_\mathrm{i}^{\perp}}{\omega} & 0 & -\beta^{(1)} & -\beta^{(2)}\\ 0 & \frac{ck_\mathrm{i}^{\perp}}{\omega} & 1 & 1\\ 0 & -1 & \gamma^{(1)} & \gamma^{(2)}\end{pmatrix}, \tag{A23}$$

$$\mathbf{M}_2 = \begin{pmatrix}-1 & 1 & \alpha^{(1)} & \alpha^{(2)}\\ \frac{ck_\mathrm{i}^{\perp}}{\omega} & \frac{ck_\mathrm{i}^{\perp}}{\omega} & -\beta^{(1)} & -\beta^{(2)}\\ 0 & 0 & 1 & 1\\ 0 & 0 & \gamma^{(1)} & \gamma^{(2)}\end{pmatrix}, \tag{A24}$$

$$\mathbf{M}_3 = \begin{pmatrix}0 & 0 & \alpha^{(1)} & \alpha^{(2)}\\ 0 & 0 & -\beta^{(1)} & -\beta^{(2)}\\ \frac{ck_\mathrm{i}^{\perp}}{\omega} & \frac{ck_\mathrm{i}^{\perp}}{\omega} & 1 & 1\\ 1 & -1 & \gamma^{(1)} & \gamma^{(2)}\end{pmatrix}, \tag{A25}$$

$$\mathbf{M}_4 = \begin{pmatrix}-1 & 0 & \alpha^{(1)} & \alpha^{(2)}\\ \frac{ck_\mathrm{i}^{\perp}}{\omega} & 0 & -\beta^{(1)} & -\beta^{(2)}\\ 0 & \frac{ck_\mathrm{i}^{\perp}}{\omega} & 1 & 1\\ 0 & 1 & \gamma^{(1)} & \gamma^{(2)}\end{pmatrix}. \tag{A26}$$

Having found the reflection coefficients for waves reflected at body 1 ($\mathscr{R}^{+}$), we can easily derive the ones reflected by body 2 ($\mathscr{R}^{-}$). To this end one simply has to invert the direction of the z coordinate ($z \to -z$) and therefore replace $\epsilon_{yz} \to -\epsilon_{yz}$, $k_z \to -k_z$, and $k_z^{(m)} \to -k_z^{(m)}$. Thus we have

$$r_{\sigma\sigma'}^{-} = r_{\sigma\sigma'}^{+}|_{\epsilon_{yz}\to-\epsilon_{yz},\ k_z\to-k_z,\ k_z^{(m)}\to-k_z^{(m)}}. \tag{A27}$$

We also want to calculate the reflection coefficients in the nonretarded limit by assuming $k^{\parallel} \gg \omega/c$. In this limit we find from Eqs. (A19), (A20), (A21), (A22), and (A27)

$$r_{\mathrm{s,s}}^{\pm} \simeq r_{\mathrm{s,p}}^{\pm} \simeq r_{\mathrm{p,s}}^{\pm} \simeq 0, \tag{A28}$$

$$r_{\mathrm{pp}}^{\pm}(\omega) \simeq \frac{-2 + D \mp 2i\epsilon_{yz}\sin(\Phi^{\pm} - \varphi)}{2 + D \mp 2i\epsilon_{yz}\sin(\Phi^{\pm} - \varphi)}, \tag{A29}$$

$$D = \sqrt{2\epsilon_{zz}\{\epsilon_{zz} + \epsilon_{\mathrm{xx}} + (\epsilon_{\mathrm{xx}} - \epsilon_{zz})\cos[2(\Phi^{\pm} - \varphi)]\}}. \tag{A30}$$

Finally, we can insert the results for the reflection coefficients found in Eqs. (A19), (A20), (A21), (A22), and (A27) into Eq. (A1) to find a fully analytic expression for the Green's tensor of our setup. In the next section we want to use this result to calculate the Casimir force.

APPENDIX B: CASIMIR FORCE BETWEEN TWO INFINITE HALF-SPACES OF A PTI

The starting point for the calculation of the Casimir force between two infinite half-spaces of a PTI separated by a layer

of vacuum of thickness L can be found in Eq. (18) of [35]:

$$\mathbf{F} = -\frac{\hbar}{2\pi}\int_0^\infty d\xi \int_{\partial V} d\mathbf{A}\cdot\Bigg(\underbrace{\left\{\frac{2\xi^2}{c^2}\mathscr{S}[\mathbf{G}^{(1)}(\mathbf{r},\mathbf{r}',i\xi)] + 2\nabla\times\mathscr{S}[\mathbf{G}^{(1)}(\mathbf{r},\mathbf{r}',i\xi)]\times\overleftarrow{\nabla}'\right\}_{\mathbf{r}'\to\mathbf{r}}}_{\equiv\,\mathbf{S}^{(1)}(\mathbf{r},i\xi)}$$
$$-\mathrm{Tr}\left[\frac{\xi^2}{c^2}\mathbf{G}^{(1)}(\mathbf{r},\mathbf{r}',i\xi) + \nabla\times\mathbf{G}^{(1)}(\mathbf{r},\mathbf{r}',i\xi)\times\overleftarrow{\nabla}'\right]_{\mathbf{r}'\to\mathbf{r}}\mathbf{I}\Bigg). \tag{B1}$$

Here ∂V is any infinite planar surface in the vacuum gap between the two planar bodies, and $d\mathbf{A}$ is its surface element, whose sign depends on the body on which $\mathbf{F}$ acts. First, we want to calculate the 3×3 tensor $\mathbf{S}^{(1)}(\mathbf{r},i\xi)$ from whose entries $S^{(1)}_{ij}(\mathbf{r},i\xi)$ we obtain the surface force density $\mathbf{f}$ acting on body 1 using Eq. (B1) via

$$\mathbf{f} = \frac{\hbar}{2\pi}\int_0^\infty d\xi\,\frac{1}{2}\big[S^{(1)}_{zz}(\mathbf{r},i\xi) - S^{(1)}_{xx}(\mathbf{r},i\xi) - S^{(1)}_{yy}(\mathbf{r},i\xi)\big]\mathbf{e}_z + S^{(1)}_{zx}(\mathbf{r},i\xi)\mathbf{e}_x + S^{(1)}_{zy}(\mathbf{r},i\xi)\mathbf{e}_y, \tag{B2}$$

where we used $d\mathbf{A} = -dA\mathbf{e}_z$. To find $\mathbf{S}^{(1)}(\mathbf{r},i\xi)$ we are going to calculate its different components step by step. That means, in the following, we are going to calculate $\mathbf{G}^{(1)T}(\mathbf{r}',\mathbf{r},\omega)$, $\mathbf{G}^{(1)}(\mathbf{r},\mathbf{r}',\omega)+\mathbf{G}^{(1)T}(\mathbf{r}',\mathbf{r},\omega)$, and $\nabla\times[\mathbf{G}^{(1)}(\mathbf{r},\mathbf{r}',\omega)+\mathbf{G}^{(1)T}(\mathbf{r}',\mathbf{r},\omega)]\times\overleftarrow{\nabla}'$ subsequently.

First, we rewrite the Green's tensor given in Eq. (A1) by inserting the reflection matrices as found in Eq. (A5) and expanding the scalar products to obtain

$$\mathbf{G}^{(1)}(\mathbf{r},\mathbf{r}',\omega) = \frac{1}{8\pi^2}\int d^2\mathbf{k}^\parallel \frac{e^{i\mathbf{k}^\parallel\cdot(\mathbf{r}-\mathbf{r}')}}{\kappa}\sum_{\sigma,\sigma'}\Bigg[\mathbf{e}^\sigma_+\mathbf{e}^{\sigma'}_- e e^{-\kappa(z+z')}\underbrace{\sum_{\sigma_1}\frac{r^-_{\sigma\sigma_1}}{D^+_{\sigma_1\sigma'}}}_{\equiv \mathrm{I}_{\sigma\sigma'}(\mathbf{k}^\parallel)} + \mathbf{e}^\sigma_-\mathbf{e}^{\sigma'}_+ e^{\kappa(z+z')}e^{-2\kappa L}\underbrace{\sum_{\sigma_1}\frac{r^+_{\sigma\sigma_1}}{D^-_{\sigma_1\sigma'}}}_{\equiv \mathrm{II}_{\sigma\sigma'}(\mathbf{k}^\parallel)}$$
$$+\mathbf{e}^\sigma_+\mathbf{e}^{\sigma'}_+ e^{-\kappa(z-z'+2L)}\underbrace{\sum_{\sigma_1,\sigma_2}\frac{r^-_{\sigma\sigma_1}r^+_{\sigma_2\sigma'}}{D^+_{\sigma_1\sigma_2}}}_{\equiv \mathrm{III}_{\sigma\sigma'}(\mathbf{k}^\parallel)} + \mathbf{e}^\sigma_-\mathbf{e}^{\sigma'}_- e^{-\kappa(z'-z+2L)}\underbrace{\sum_{\sigma_1,\sigma_2}\frac{r^+_{\sigma\sigma_1}r^-_{\sigma_2\sigma'}}{D^-_{\sigma_1\sigma_2}}}_{\mathrm{IV}_{\sigma\sigma'}(\mathbf{k}^\parallel)}\Bigg]. \tag{B3}$$

Here we have replaced $k_z = i\kappa$, and the polarization indices are σ, σ', σ_1, $\sigma_2 = s, p$. Furthermore, $D^\pm_{\sigma_1\sigma_2} = (\mathscr{D}^\pm)_{\sigma_1\sigma_2}$ refers to components of the matrix $\mathscr{D}^\pm$ defined in Eq. (A4).

To obtain $\mathbf{S}^{(1)}(\mathbf{r},i\xi)$, in the second step, we calculate $\mathbf{G}^{(1)\mathrm{T}}(\mathbf{r}',\mathbf{r},i\xi)$. Because of the switching of $\mathbf{r}'$ and $\mathbf{r}$ we have to substitute $\mathbf{k}^\parallel\to-\mathbf{k}^\parallel$ to ensure that the term $e^{i\mathbf{k}^\parallel\cdot(\mathbf{r}-\mathbf{r}')}$ stays the same. Using the fact that $\mathbf{e}^\pm_p\to\mathbf{e}^\mp_p$ and $\mathbf{e}^\pm_s\to-\mathbf{e}^\pm_s=-\mathbf{e}^\mp_s$ for $\mathbf{k}^\parallel\to-\mathbf{k}^\parallel$, we therefore get

$$\mathbf{G}^{(1)\mathrm{T}}(\mathbf{r}',\mathbf{r},i\xi) = \frac{1}{8\pi^2}\int d^2\mathbf{k}^\parallel\frac{e^{i\mathbf{k}^\parallel\cdot(\mathbf{r}-\mathbf{r}')}}{\kappa}\sum_{\sigma,\sigma'}\{(-1)^{\sigma\sigma'}[\mathbf{e}^\sigma_+\mathbf{e}^{\sigma'}_- e^{-\kappa(z+z')}\,\mathrm{I}_{\sigma'\sigma}(-\mathbf{k}^\parallel) + \mathbf{e}^\sigma_-\mathbf{e}^{\sigma'}_+ e^{\kappa(z+z'-2L)}\,\mathrm{II}_{\sigma'\sigma}(-\mathbf{k}^\parallel)$$
$$+\mathbf{e}^\sigma_-\mathbf{e}^{\sigma'}_- e^{-\kappa(z'-z+2L)}\,\mathrm{III}_{\sigma'\sigma}(-\mathbf{k}^\parallel) + \mathbf{e}^\sigma_+\mathbf{e}^{\sigma'}_+ e^{\kappa(z'-z-2L)}\,\mathrm{IV}_{\sigma'\sigma}(-\mathbf{k}^\parallel)]\}. \tag{B4}$$

Here we also relabel $\sigma\leftrightarrow\sigma'$ and introduce $(-1)^{\sigma\sigma'}$, given by

$$(-1)^{\sigma\sigma'} = \begin{cases} 1 & \text{if } \sigma = \sigma', \\ -1 & \text{if } \sigma\neq\sigma'. \end{cases} \tag{B5}$$

As a side note, we want to mention here that by comparing Eqs. (B3) and (B4), one finds that Onsager's reciprocity, i.e., $\mathbf{G}^{(1)\mathrm{T}}(\mathbf{r}',\mathbf{r},i\xi) = \mathbf{G}^{(1)}(\mathbf{r},\mathbf{r}',i\xi)$, holds if

$$(-1)^{\sigma\sigma'}R_{\sigma'\sigma}(-\mathbf{k}^\parallel) = R_{\sigma\sigma'}(\mathbf{k}^\parallel), \quad R = \mathrm{I},\mathrm{II},\mathrm{III},\mathrm{IV}. \tag{B6}$$

Note that a similar expression has also been found in Ref. [39] for one-dimensional nanogratings. Nevertheless, in the setup considered here Eq. (B6) is not satisfied, and hence Onsager reciprocity is violated. Continuing with finding an expression for

$\mathbf{S}^{(1)}(\mathbf{r}, i\xi)$, we combine Eqs. (B3) and (B4) and obtain

$$\begin{aligned}\mathbf{G}^{(1)}(\mathbf{r},\mathbf{r}',i\xi)+\mathbf{G}^{(1)\mathrm{T}}(\mathbf{r}',\mathbf{r},i\xi) = \frac{1}{8\pi^2}\int d^2\mathbf{k}^{\parallel}\frac{e^{i\mathbf{k}^{\parallel}\cdot(\mathbf{r}-\mathbf{r}')}}{\kappa}\sum_{\sigma,\sigma'}\{&\mathbf{e}_+^{\sigma}\mathbf{e}_-^{\sigma'}e^{-\kappa(z+z')}\left[(-1)^{\sigma\sigma'}\mathrm{I}_{\sigma'\sigma}(-\mathbf{k}^{\parallel})+\mathrm{I}_{\sigma\sigma'}(\mathbf{k}^{\parallel})\right]\\ &+\mathbf{e}_-^{\sigma}\mathbf{e}_+^{\sigma'}e^{\kappa(z+z'-2L)}\left[(-1)^{\sigma\sigma'}\mathrm{II}_{\sigma'\sigma}(-\mathbf{k}^{\parallel})+\mathrm{II}_{\sigma\sigma'}(\mathbf{k}^{\parallel})\right]\\ &+\mathbf{e}_-^{\sigma}\mathbf{e}_-^{\sigma'}e^{-\kappa(z'-z+2L)}\left[(-1)^{\sigma\sigma'}\mathrm{III}_{\sigma'\sigma}(-\mathbf{k}^{\parallel})+\mathrm{III}_{\sigma\sigma'}(\mathbf{k}^{\parallel})\right]\\ &+\mathbf{e}_+^{\sigma}\mathbf{e}_+^{\sigma'}e^{\kappa(z'-z-2L)}\left[(-1)^{\sigma\sigma'}\mathrm{IV}_{\sigma'\sigma}(-\mathbf{k}^{\parallel})+\mathrm{IV}_{\sigma\sigma'}(\mathbf{k}^{\parallel})\right]\}.\end{aligned} \tag{B7}$$

Next, we need to evaluate the curls. This can be done by realizing that the operators ∇ and $\overleftarrow{\nabla}$ reduce to $\nabla \to i\mathbf{k}_{\pm}$ and $\overleftarrow{\nabla} \to -i\mathbf{k}_{\pm}$, where $\mathbf{k}_{\pm} = \mathbf{k}^{\parallel} \pm i\kappa\mathbf{e}_z$. Using $i\mathbf{k}_{\pm}\times\mathbf{e}_{\mathrm{s}\pm} = \frac{\xi}{c}\mathbf{e}_{\mathrm{p}\pm}$, $i\mathbf{k}_{\pm}\times\mathbf{e}_{\mathrm{p}\pm} = -\frac{\xi}{c}\mathbf{e}_{\mathrm{s}\pm}$, we find that $\nabla\times\mathscr{S}[\mathbf{G}^{(1)}(\mathbf{r},\mathbf{r}',i\xi)]\times\overleftarrow{\nabla}'$ is obtained from $\mathscr{S}[\mathbf{G}^{(1)}(\mathbf{r},\mathbf{r}',i\xi)]$ by simply replacing all $\mathbf{e}_{\pm}^{\sigma\sigma'} \to \mathbf{e}_{\pm}^{\bar{\sigma}\bar{\sigma}'}\xi^2(-1)^{\sigma\sigma'}/c^2$, where $\bar{\sigma}$ is defined by $\bar{s} = p$ and $\bar{p} = s$. We can combine this result with Eq. (B7) to find

$$\begin{aligned}\mathbf{S}^{(1)}(\mathbf{r},i\xi) = \frac{\xi^2}{8\pi^2c^2}\int d^2\mathbf{k}^{\parallel}\frac{e^{i\mathbf{k}^{\parallel}\cdot(\mathbf{r}-\mathbf{r}')}}{\kappa}\sum_{\sigma,\sigma'}\{&\underbrace{[\mathbf{e}_+^{\sigma}\mathbf{e}_-^{\sigma'}+\mathbf{e}_-^{\sigma'}\mathbf{e}_+^{\sigma}+(-1)^{\sigma\sigma'}(\mathbf{e}_+^{\bar{\sigma}}\mathbf{e}_-^{\bar{\sigma}'}+\mathbf{e}_-^{\bar{\sigma}'}\mathbf{e}_+^{\bar{\sigma}})]}_{\equiv\mathbf{Q}^{(1)}}[e^{-2\kappa z}\mathrm{I}_{\sigma\sigma'}(\mathbf{k}^{\parallel})+e^{2\kappa(z-L)}\mathrm{II}_{\sigma'\sigma}(\mathbf{k}^{\parallel})]\\ &+e^{-2\kappa L}\underbrace{[\mathbf{e}_-^{\sigma}\mathbf{e}_-^{\sigma'}+\mathbf{e}_+^{\sigma'}\mathbf{e}_+^{\sigma}+(-1)^{\sigma\sigma'}(\mathbf{e}_-^{\bar{\sigma}}\mathbf{e}_-^{\bar{\sigma}'}+\mathbf{e}_+^{\bar{\sigma}'}\mathbf{e}_+^{\bar{\sigma}})]}_{\equiv\mathbf{Q}^{(2)}}[\mathrm{III}_{\sigma\sigma'}(\mathbf{k}^{\parallel})+\mathrm{IV}_{\sigma'\sigma}(\mathbf{k}^{\parallel})]\}.\end{aligned} \tag{B8}$$

Here, in the last step, we substituted $\mathbf{k}^{\parallel} \to -\mathbf{k}^{\parallel}$ back in some of the terms to find the two tensor valued prefactors $\mathbf{Q}^{(1)}$ and $\mathbf{Q}^{(2)}$ corresponding to terms with odd and even numbers of reflections, respectively. To eventually be able to evaluate Eq. (B2) we need to calculate the outer products in $\mathbf{Q}^{(1)}$ and $\mathbf{Q}^{(2)}$ in Cartesian coordinates. With the help of Eq. (A2) we find

$$\mathbf{e}_+^{\mathrm{p}}\mathbf{e}_{\pm}^{\mathrm{p}} = \frac{c^2}{\xi^2(k^{\parallel})^2}\begin{pmatrix}-\kappa^2k_x^2 & -\kappa^2k_xk_y & \pm i(k^{\parallel})^2\kappa k_x\\ -\kappa^2k_xk_y & -\kappa^2k_y^2 & \pm i(k^{\parallel})^2\kappa k_y\\ \mp i(k^{\parallel})^2\kappa k_x & \mp i(k^{\parallel})^2\kappa k_y & -(k^{\parallel})^4\end{pmatrix}, \tag{B9}$$

$$\mathbf{e}_-^{\mathrm{p}}\mathbf{e}_{\pm}^{\mathrm{p}} = \frac{c^2}{\xi^2(k^{\parallel})^2}\begin{pmatrix}\kappa^2k_x^2 & \kappa^2k_xk_y & \pm i(k^{\parallel})^2\kappa k_x\\ \kappa^2k_xk_y & \kappa^2k_y^2 & \pm i(k^{\parallel})^2\kappa k_y\\ \pm i(k^{\parallel})^2\kappa k_x & \pm i(k^{\parallel})^2\kappa k_y & -(k^{\parallel})^4\end{pmatrix}, \tag{B10}$$

$$\mathbf{e}_{\pm}^{\mathrm{s}}\mathbf{e}_{\pm}^{\mathrm{s}} = \mathbf{e}_{\pm}^{\mathrm{s}}\mathbf{e}_{\mp}^{\mathrm{s}} = \frac{1}{(k^{\parallel})^2}\begin{pmatrix}k_y^2 & -k_xk_y & 0\\ -k_xk_y & k_x^2 & 0\\ 0 & 0 & 0\end{pmatrix}, \tag{B11}$$

$$\mathbf{e}_+^{\mathrm{s}}\mathbf{e}_{\pm}^{\mathrm{p}} = \mathbf{e}_-^{\mathrm{s}}\mathbf{e}_{\pm}^{\mathrm{p}} = (\mathbf{e}_{\pm}^{\mathrm{s}}\mathbf{e}_+^{\mathrm{s}})^{\mathrm{T}} = (\mathbf{e}_{\pm}^{\mathrm{p}}\mathbf{e}_-^{\mathrm{s}})^{\mathrm{T}} \tag{B12}$$

$$= \frac{c}{\xi(k^{\parallel})^2}\begin{pmatrix}\mp\kappa k_xk_y & \mp\kappa k_y^2 & i(k^{\parallel})^2k_y\\ \pm\kappa k_x^2 & \pm\kappa k_xk_y & -i(k^{\parallel})^2k_x\\ 0 & 0 & 0\end{pmatrix}. \tag{B13}$$

Comparing Eq. (B8) with Eq. (B2), we see that we need to evaluate the terms $(Q_{zz}^{(i)} - Q_{xx}^{(i)} - Q_{yy}^{(i)})/2$, $Q_{zx}^{(i)}$, and $Q_{zy}^{(i)}$. Using Eqs. (B9)–(B13) and the dispersion relation $(k^{\parallel})^2 - \kappa^2 = -\xi^2/c^2$, we eventually find

$$\left(Q_{zz}^{(1)} - Q_{xx}^{(1)} - Q_{yy}^{(1)}\right)/2 = Q_{zx}^{(1)} = Q_{zy}^{(1)} = 0, \tag{B14}$$

$$Q_{zx}^{(2)} = Q_{zy}^{(2)} = 0, \tag{B15}$$

$$\left(Q_{zz}^{(2)} - Q_{xx}^{(2)} - Q_{yy}^{(2)}\right)/2 = -\frac{2c^2}{\xi^2}\kappa^2. \tag{B16}$$

Equation (B14) shows that all terms with an odd number of reflections do not contribute to the Casimir force, whereas Eq. (B15) tells us that there is no lateral Casimir force, i.e., a nonzero x or y component of $\mathbf{f}$. Finally, using Eqs. (B2), (B8), and

(B14)–(B16), we find the final result for the Casimir force density acting on body 1:

$$\mathbf{f} = -\frac{\hbar}{8\pi^3}\int_0^\infty d\xi \int d^2\mathbf{k}^\parallel \kappa e^{-2\kappa L}[\mathrm{III}_{pp}(\mathbf{k}^\parallel) + \mathrm{IV}_{pp}(\mathbf{k}^\parallel) + \mathrm{III}_{ss}(\mathbf{k}^\parallel) + \mathrm{IV}_{ss}(\mathbf{k}^\parallel)]\mathbf{e}_z \tag{B17}$$

$$= -\frac{\hbar}{8\pi^3}\int_0^\infty d\xi \int_0^{2\pi} d\varphi \int_0^\infty dk^\parallel \kappa e^{-2\kappa L}\mathrm{Tr}[\mathscr{R}^- \cdot (\mathscr{D}^+)^{-1} \cdot \mathscr{R}^+ + \mathscr{R}^+ \cdot (\mathscr{D}^-)^{-1} \cdot \mathscr{R}^-]\mathbf{e}_z. \tag{B18}$$

Note that this result differs from the one obtained in Ref. [35] only by the fact that in Eq. (B18) we cannot carry out the $d\varphi$ integral due to the φ dependence of the reflection coefficients, whereas in Ref. [35] the media were isotropic in the plane of the surfaces and hence this integral simply gave a factor of 2π.

In the nonretarded limit the reflection coefficients simplify significantly according to Eqs. (A28) and (A30), and thus Eq. (B18) reduces to

$$\mathbf{f} = -\frac{\hbar}{16\pi^3 L^3}\int_0^\infty d\xi \int_0^{2\pi} d\varphi \int_0^\infty d\kappa\, \kappa^2 \frac{r_{\mathrm{pp}}^+(i\xi)r_{\mathrm{pp}}^-(i\xi)e^{-2\kappa L}}{1 - r_{\mathrm{pp}}^+(i\xi)r_{\mathrm{pp}}^-(i\xi)e^{-2\kappa L}}\mathbf{e}_z$$

$$= -\frac{\hbar}{16\pi^3 L^3}\int_0^\infty d\xi \int_0^{2\pi} d\varphi\ \mathrm{Li}_3[r_{\mathrm{pp}}^+(i\xi)r_{\mathrm{pp}}^-(i\xi)]\mathbf{e}_z. \tag{B19}$$

[1] H. B. G. Casimir, Proc. K. Ned. Akad. Wet. **51**, 793 (1948).
[2] I. E. Dzyaloshinskii, E. M. Lifshitz, and L. P. Pitaevskii, Adv. Phys. **10**, 165 (1961).
[3] S. J. van Enk, Phys. Rev. A **52**, 2569 (1995).
[4] F. S. S. Rosa, D. A. R. Dalvit, and P. W. Milonni, Phys. Rev. A **78**, 032117 (2008).
[5] R. B. Rodrigues, P. A. M. Neto, A. Lambrecht, and S. Reynaud, Europhys. Lett. **76**, 822 (2006).
[6] Y. S. Barash, Radiophys. Quantum Electron. (Engl. Transl.) **21**, 1138 (1978).
[7] T. G. Philbin and U. Leonhardt, Phys. Rev. A **78**, 042107 (2008).
[8] J. C. Torres-Guzmán and W. L. Mochán, J. Phys. A **39**, 6791 (2006).
[9] P. Thiyam, P. Parashar, K. V. Shajesh, O. I. Malyi, M. Boström, K. A. Milton, I. Brevik and C. Persson, Phys. Rev. Lett. **120**, 131601 (2018).
[10] F. Chen, U. Mohideen, G. L. Klimchitskaya, and V. M. Mostepanenko, Phys. Rev. Lett. **88**, 101801 (2002).
[11] F. Chen, U. Mohideen, G. L. Klimchitskaya, and V. M. Mostepanenko, Phys. Rev. A **66**, 032113 (2002).
[12] F. Chen, B. Harris, A. Roy, and U. Mohideen, Int. J. Mod. Phys. A **17**, 711 (2002).
[13] H. C. Chiu, G. L. Klimchitskaya, V. N. Marachevsky, V. M. Mostepanenko, and U. Mohideen, Phys. Rev. B **80**, 121402 (2009).
[14] H. C. Chiu, G. L. Klimchitskaya, V. N. Marachevsky, V. M. Mostepanenko, and U. Mohideen, Phys. Rev. B **81**, 115417 (2010).
[15] J. N. Munday, D. Iannuzzi, Y. Barash, and F. Capasso, Phys. Rev. A **71**, 042102 (2005).
[16] D. Iannuzzi, M. Lisanti, J. N. Munday, and F. Capasso, Solid State Commun. **135**, 618 (2005).
[17] X. Chen and J. C. H. Spence, Phys. Status Solidi B **248**, 2064 (2011).
[18] M. Z. Hasan and C. L. Kane, Rev. Mod. Phys. **82**, 3045 (2010).
[19] S. Raghu and F. D. M. Haldane, Phys. Rev. A **78**, 033834 (2008).
[20] S. A. Hassani Gangaraj, M. G. Silveirinha, and G. W. Hanson, IEEE J. Multiscale Multiphys. Comput. Tech. **2**, 3 (2017).
[21] L. Lu, J. D. Joannopoulos, and M. Soljačić, Nat. Photonics **8**, 821 (2014).
[22] A. B. Khanikaev, S. Hossein Mousavi, W.-K. Tse, M. Kargarian, A. H. MacDonald, and G. Shvets, Nat. Mater. **12**, 233 (2012).
[23] W. Gao, B. Yang, M. Lawrence, F. Fang, B. Béri, and S. Zhang, Nat. Commun. **7**, 12435 (2016).
[24] M. G. Silveirinha, Phys. Rev. B **92**, 125153 (2015).
[25] M. G. Silveirinha, Phys. Rev. B **94**, 205105 (2016).
[26] A. R. Davoyan and N. Engheta, Phys. Rev. Lett. **111**, 257401 (2013).
[27] F. D. M. Haldane and S. Raghu, Phys. Rev. Lett. **100**, 013904 (2008).
[28] S. A. H. Gangaraj, G. W. Hanson, and M. Antezza, Phys. Rev. A **95**, 063807 (2017).
[29] M. G. Silveirinha, S. A. Gangaraj, G. W. Hanson, and M. Antezza, Phys. Rev. A **97**, 022509 (2018).
[30] S. A. H. Gangaraj, G. W. Hanson, M. Antezza, and M. G. Silveirinha, Phys. Rev. B **97**, 201108(R) (2018).
[31] S. A. H. Gangaraj, M. G. Silveirinha, G. W. Hanson, M. Antezza, and F. Monticone, Phys. Rev. B **98**, 125146 (2018).
[32] R. M. Abraham Ekeroth, P. Ben-Abdallah, J. C. Cuevas, and A. García-Martín, ACS Photonics **5**, 705 (2018).
[33] L. Zhu and S. Fan, Phys. Rev. Lett. **117**, 134303 (2016).
[34] M. G. Silveirinha, Phys. Rev. B **95**, 115103 (2017).
[35] S. Fuchs, F. Lindel, R. V. Krems, G. W. Hanson, M. Antezza, and S. Y. Buhmann, Phys. Rev. A **96**, 062505 (2017).
[36] E. D. Palik, R. Kaplan, R. W. Gammon, H. Kaplan, R. F. Wallis, and J. J. Quinn, Phys. Rev. B **13**, 2497 (1976).
[37] S. Y. Buhmann, D. T. Butcher, and S. Scheel, New J. Phys. **14**, 083034 (2012).
[38] S. Y. Buhmann, *Dispersion Forces: Many-Body Effects, Excited Atoms, Finite Temperature and Quantum Friction* (Springer, Heidelberg, 2012).
[39] S. Y. Buhmann, V. N. Marachevsky, and S. Scheel, Int. J. Mod. Phys. A **31**, 1641029 (2016).

[40] L. Bergstrom, Adv. Colloid Interface Sci. **70**, 125 (1997).
[41] C. Henkel, K. Joulain, J.-P. Mulet, and J.-J. Greffet, Phys. Rev. A **69**, 023808 (2004).
[42] T. B. Bateman, H. J. McSkimin, and J. M. Whelan, J. Appl. Phys. **30**, 544 (1959).
[43] A. G. Grushin, P. Rodriguez-Lopez, and A. Cortijo, Phys. Rev. B **84**, 045119 (2011).
[44] T. Osaka, M. Dakai, K. Hayashi, K. Ohashi, M. Saito, and K. Yamada, Nature (London) **392**, 796 (1998).
[45] X. L. Qi, T. L. Hughes, and S. C. Zhang, Phys. Rev. B **78**, 195424 (2008).
[46] X. L. Qi, R. Li, J. Zang, and S. C. Zhang, Science **323**, 1184 (2009).
[47] K. Kim, X. Xu, J. Guo, and D. L. Fan, Nat. Commun. **5**, 3632 (2014).